Electronic Supplementary Information (ESI)

Suppression of Self-Discharge in Solid-State Supercapacitors Using a Zwitterionic Gel Electrolyte

Kangkang Ge and Guangming Liu*

Hefei National Laboratory for Physical Sciences at the Microscale, Key Laboratory of Surface and Interface Chemistry and Energy Catalysis of Anhui Higher Education Institutes, Department of Chemical Physics, University of Science and Technology of China, Hefei 230026, China.

Materials and methods

Materials.

Propylsulfonate dimethylammonium propylmethacrylamide (PDP) (≥98%, Changzhou YiPinTang Chemical Co. Ltd.) and 4,4'-azobis(4-cyanovaleric acid) (ACVA) (≥98%, Aladdin) were used as received. Polyvinyl alcohol (PVA) with a number-average molecular weight (M_n) of ~ 7.8×10^4 g mol^{-1} and lithium chloride monohydrate (LiCl·H$_2$O) were purchased from Sinopharm and used as received.

Preparation of electrolytes.

PPDP was synthesized according to the procedure reported previously.[S1] Briefly, 1.0 g PDP, 1.0 mg 4,4'-azobis(4-cyanovaleric acid) (ACVA), and 4.0 mL water were added into a round-bottom reactor. After three freeze-degas-thaw cycles, the free-radical polymerization was conducted at ~ 70 °C for ~ 10 h. Afterwards, the solution was cooled down to room temperature and then filtered, followed by dialysis against water. Finally, PPDP was obtained by lyophilization with a M_n of ~ 1.6×10^5 g mol^{-1}.

Fabrication of graphene electrodes and supercapacitors.

Graphene was purchased from the Sixth Element (Changzhou) Materials Technology Co., Ltd.. The graphene film was firstly prepared on a cellulose acetate membrane surface by vacuum filtration, followed by tightly pressing the graphene film onto a polyethylene terephthalate (PET) substrate. Afterwards, a graphene film was obtained by slowly peeling off the cellulose acetate membrane. The in-plane graphene electrode was prepared by scraping the film to form a channel. Finally, a supercapacitor was successfully fabricated by adding electrolyte into the channel with an infiltration time of 40 minutes. For the preparation of solid-state supercapacitors, a heat gun (~ 80 °C) was used to slowly evaporate the solvent to form the gel polymer electrolyte. In this work, the initial electrolyte solution had a composition of 10:1:1 (H$_2$O:polymer:LiCl·H$_2$O, w/w), and the mass ratio of H$_2$O:polymer:LiCl·H$_2$O changed to 1:1:1 in the gel state.

Electrochemical tests.

The electrochemical performance including cyclic voltammetry (CV), galvanostatic charge and discharge, and self-discharge of the graphene-based supercapacitors were measured in a two-electrode system using an electrochemical station (CHI 760E). The potential range of cyclic voltammetry was changed from 0 to

1.0 V. A constant current density (100 μA cm^{-2}) was applied to charge the supercapacitors to 1.0 V, and then the constant voltage of 1.0 V was held for 4800 s to further charge the supercapacitors to avoid the charge redistribution induced self-discharge.[S2,S3] Afterwards, the voltage decay of supercapacitors was recorded under an open circuit condition to study the self-discharge behavior. The supercapacitors were charged to 1.0 V and then electrochemical impedance measurements were performed under this voltage with an AC amplitude of 10 mV and a frequency range from 1 MHz to 0.1 Hz. The three-electrode electrochemical tests were conducted using the Ag/AgCl (saturated potassium chloride) electrode as a reference electrode. The electrochemical impedance measurements and three-electrode CV tests all use a Bio-logic VMP-300 electrochemical workstation. All the electrochemical tests were conducted at ~ 20 °C except for temperature dependent measurements.

Other characterization.

The rheological properties of electrolytes were measured using an Anton paar MCR302 rheometer. Storage (G') and loss (G'') moduli were measured as a function of strain with a frequency of 1 Hz at ~ 20 °C. Zeta potentials of PPDP, PVA, and the graphene electrode were measured using a zetasizer (Malvern Zetasizer Nanoseries) at ~ 20 °C. Water contact angles (WCA) on the surface of graphene electrodes were determined using a contact angle goniometer (CAM 200, KSV) at ~ 20 °C.

Fitting of self-discharge curves.

Three mechanisms for the self-discharge of EDLCs, ohmic leakage, diffusion control, and activation control, have been proposed.[S4,S5] For ohmic leakage, the relation between voltage (U) and time (t) can be described as:[S6]

$$U = U_0 \exp(\frac{-t}{RC})$$ (S1)

where U_0 is the initial potential of the charged supercapacitor, C is the capacitance, and RC is the time constant of the self-discharge process.

For the diffusion controlled mechanism, the relation between U and t can be described as:[S4]

$$U = U_0 - B\sqrt{t}$$ (S2)

where B is the diffusion parameter.

For the activation controlled mechanism, the relation between U and t can be described as: [S7]

$$U = U_0 - \frac{RT}{\alpha F} \ln \frac{\alpha F i_0}{RTC} - \frac{RT}{\alpha F} \ln(t + \frac{CK}{i_0}) \qquad \text{(S3)}$$

where α, T, R, F, i_0, and K are the charge transfer coefficient, temperature, gas constant, Faradaic constant, exchange current, and integration constant, respectively.

The change in U assuming that the three types of self-discharge mechanisms are independent can therefore be described as: [S4,S6]

$$U = U_0 \exp(\frac{-t}{RC}) - B\sqrt{t} - m - n \ln(t + \frac{CK}{i_0}) \qquad \text{(S4)}$$

where m and n are the constants correlated with the Faradaic process.

If only the contributions of diffusion control and activation control are considered, the relation between U and t can be described as: [S6]

$$U = A - B\sqrt{t} - P \ln(t + Q) \qquad \text{(S5)}$$

where A, P, and Q are the parameters related to the Faradaic process.
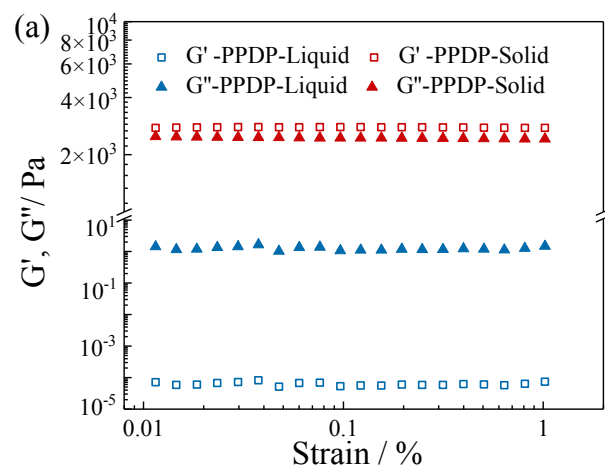
Figure S1. The PPDP electrolyte in the liquid and solid states. (a) Rheological properties of the PPDP electrolyte in the liquid and solid states. (b) Photographic illustration of the PPDP electrolyte in the liquid and solid states.
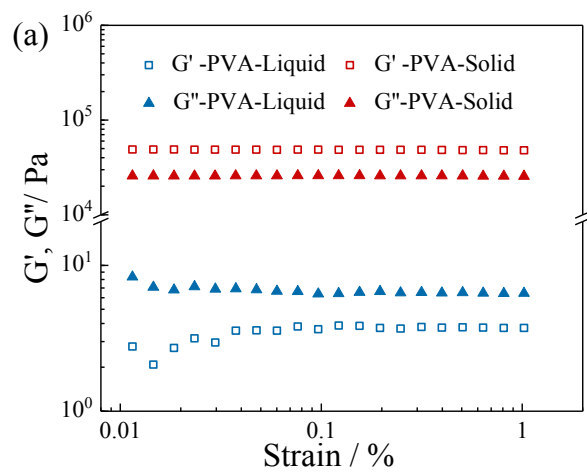
Figure S2. The PVA electrolyte in the liquid and solid states. (a) Rheological properties of the PVA electrolyte in the liquid and solid states. (b) Photographic illustration of the PVA electrolyte in the liquid and solid states.
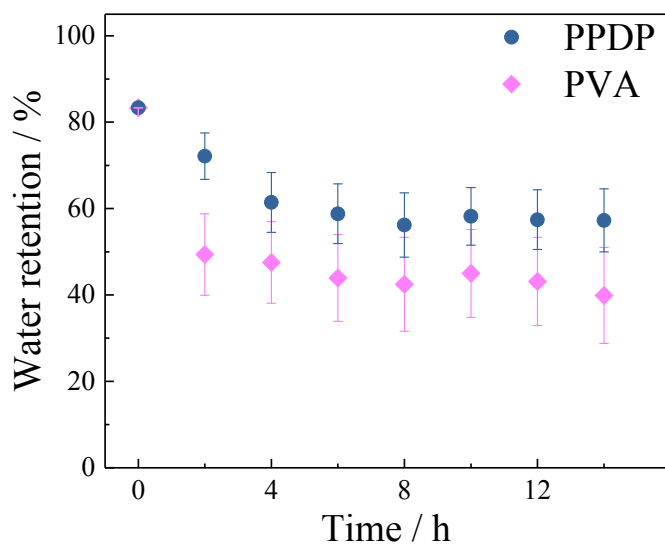
Figure S3. Water retention of the PPDP and PVA gel electrolytes as a function of time.

In Figure S3, as time increases, the water retention of the PPDP gel electrolyte is higher than that of the PVA gel electrolyte at ~ 25 °C in room environment. The high water retention ability is favorable for ion migration and cyclability of the gel polymer electrolyte based supercapacitors.
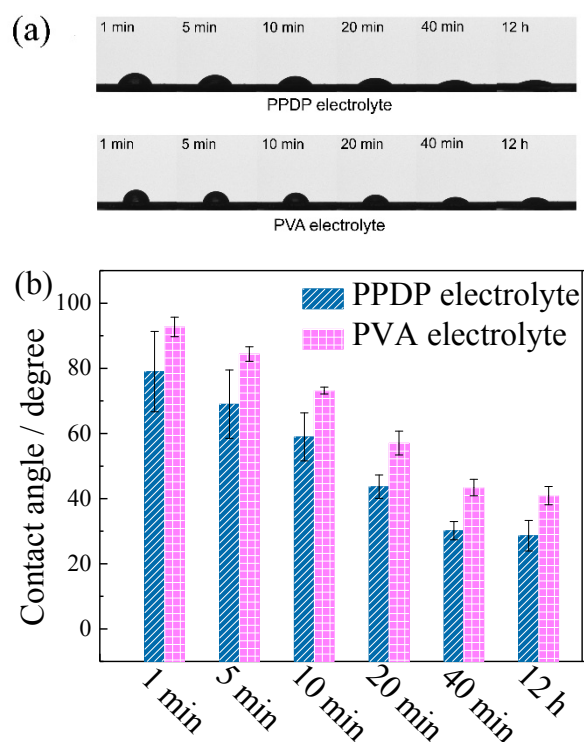
Figure S4. (a) Photographic illustration of the contact angle of PPDP and PVA electrolytes on a graphene substrate as a function of time, at 20 °C in air. (b) Contact angles of PPDP and PVA electrolytes on a graphene substrate as a function of time, at 20 °C in air.

In Figure S4, the contact angle of both PPDP and PVA electrolytes on a graphene substrate is seen to decrease with time during water evaporation. The contact angle of PPDP electrolyte is ~ 15° lower than that of PVA electrolyte at all times, indicating that the former has a better wetting behavior on the electrode surface than the later. This fact suggests that the PPDP electrolyte can more easily penetrate into the electrode, presenting a larger interfacial contact area between electrolyte and electrode. This may be because PPDP has stronger affinities with the graphene electrode than PVA (Figure S5). The electrochemical performance of SSCs strongly depends on the interfacial contact area between electrode and gel polymer electrolyte, thus, the SSC employing PPDP gel electrolyte exhibits better electrochemical performance than that employing PVA gel electrolyte.
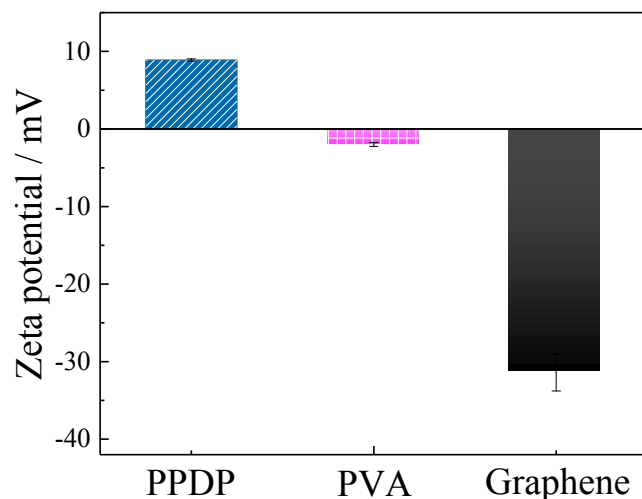
Figure S5. Zeta potentials of PPDP (0.04 mg mL^{-1}), PVA (0.04 mg mL^{-1}), and the graphene electrode in the presence of 10 mM LiCl.

As shown in Figure S5, the zeta potentials of PPDP and PVA are ~ 8.9 and ~ -1.8 mV, respectively. The positive zeta potential of zwitterionic PPDP might be attributed to the strong interactions between the positively charged Li$^+$ ions and the negatively charged sulfonate groups. On the other hand, the surface zeta potential of the graphene electrode is ~ -31.3 mV. Consequently, PPDP would have stronger affinities with the graphene electrode compared with PVA.
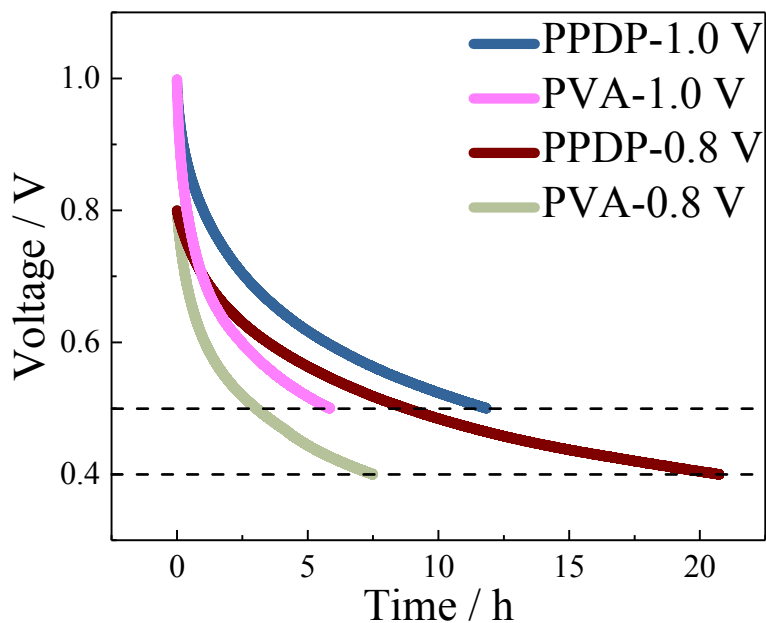
Figure S6. Time dependence of the decay of voltage of the SSCs employing PPDP or PVA gel electrolyte, where the voltage decays either from 1.0 to 0.5 V or from 0.8 to 0.4 V.

In Figure S6, the voltage decay is slower with an initial voltage of 0.8 V compared with that with an initial voltage of 1.0 V for both PPDP and PVA based SSCs, similar to the observation in the previous work.[S3] Nevertheless, the self-discharge time for half-voltage decay of the PPDP based SSC is still much longer than that of the PVA based SSC when the SSCs are charged to 0.8 V.
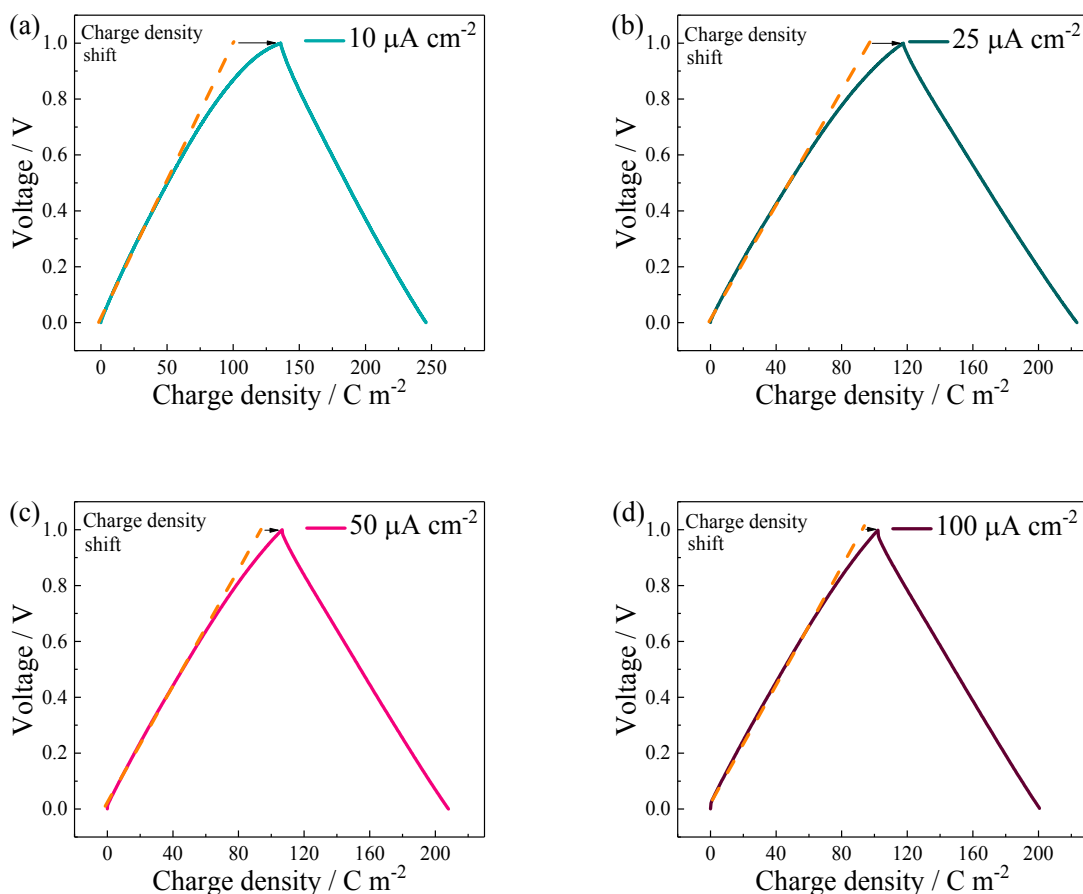
Figure S7. Galvanostatic charge-discharge curves of the SSC employing PPDP gel electrolyte in a conventional in-plane configuration. The current densities from (a) to (d) are 10, 25, 50, and 100 µA cm^{-2}, respectively. The charge-discharge time is transformed into charge density by multiplying by the current density and then the charge density is normalized to the active area of the graphene electrode. The shift in charge density can be obtained by comparing the charging curves between an ideally polarized electrode (the dashed lines) and the graphene electrode employed here.
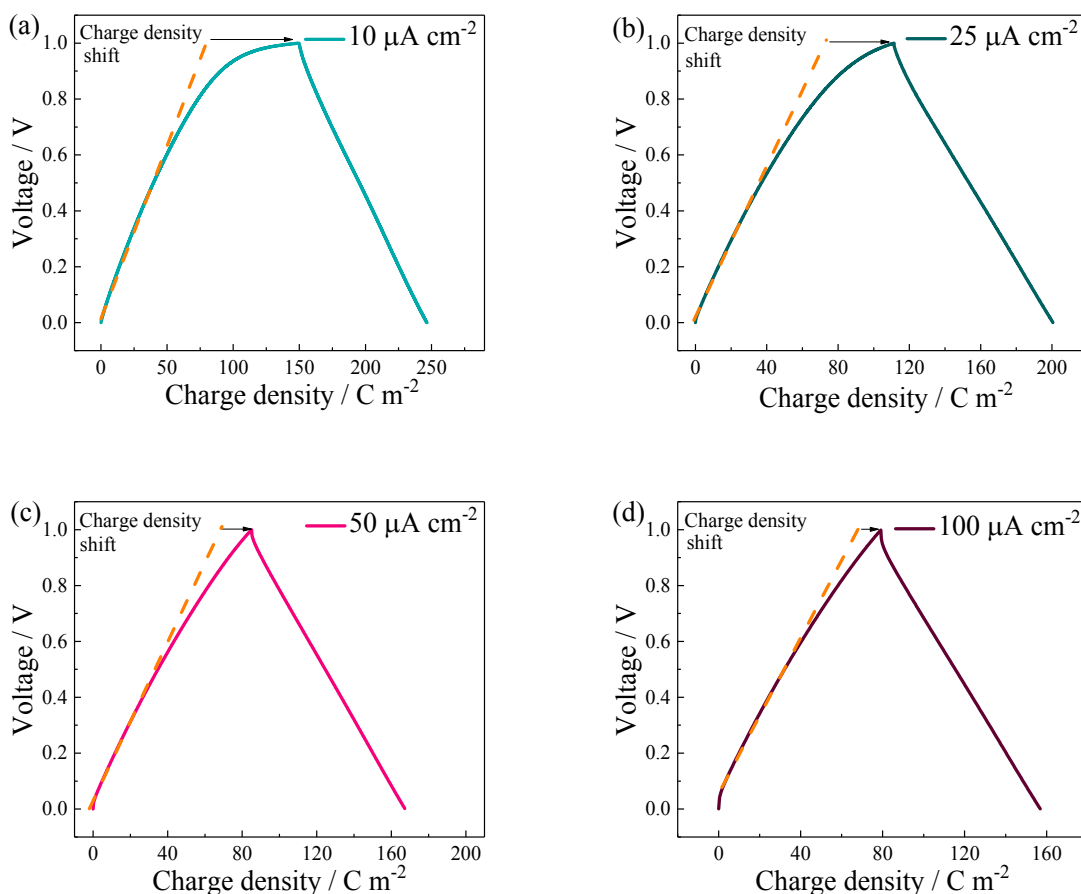
Figure S8. Galvanostatic charge-discharge curves of the SSC employing PVA gel electrolyte in a conventional in-plane configuration. The current densities from (a) to (d) are 10, 25, 50, and 100 μA cm^{-2}, respectively. The charge-discharge time is transformed into charge density by multiplying by the current density and then the charge density is normalized to the active area of the graphene electrode. The shift in charge density can be obtained by comparing the charging curves between an ideally polarized electrode (the dashed lines) and the graphene electrode employed here.
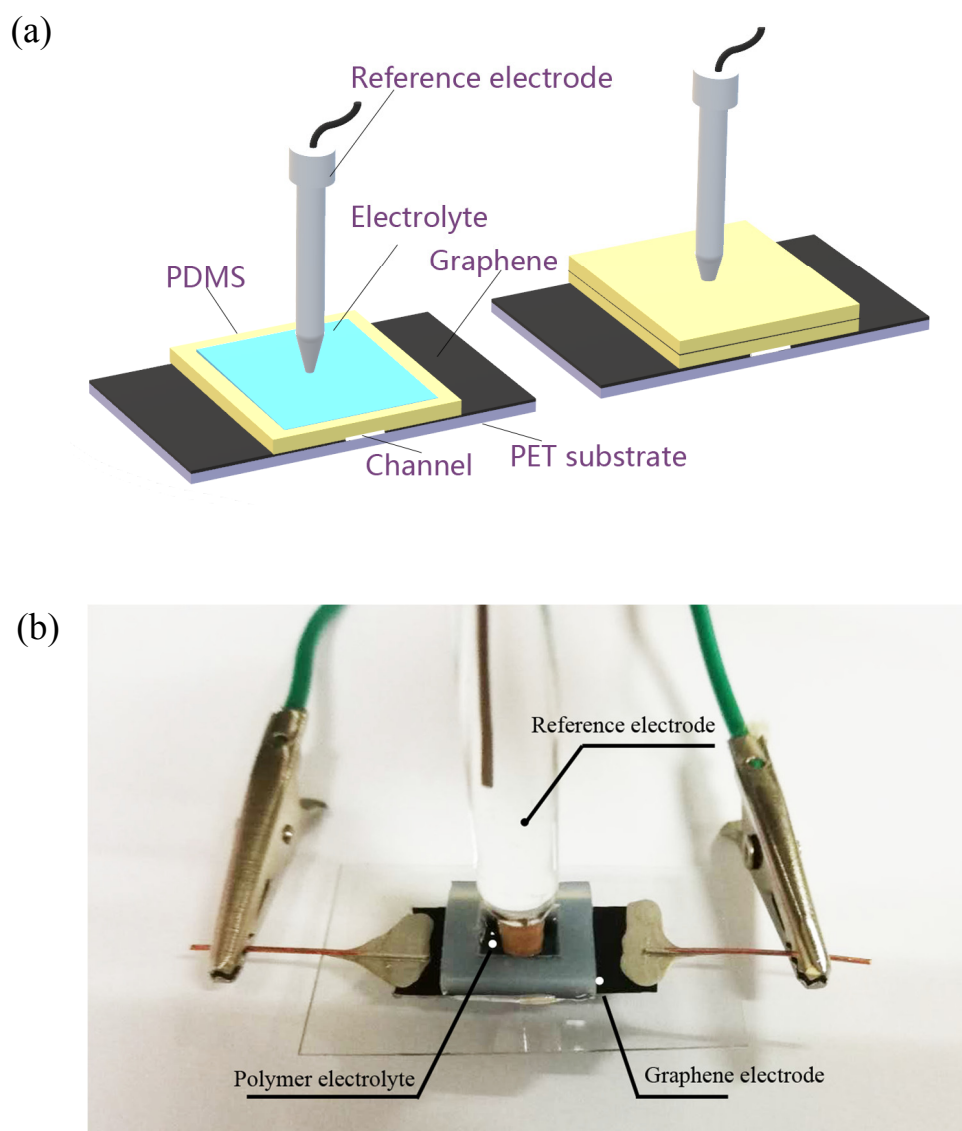
Figure S9. (a) Schematic illustration and (b) a photograph of the three-electrode test of a graphene-based in-plane supercapacitor. Here, the tip of the reference electrode is immersed into the electrolyte during the electrochemical tests.
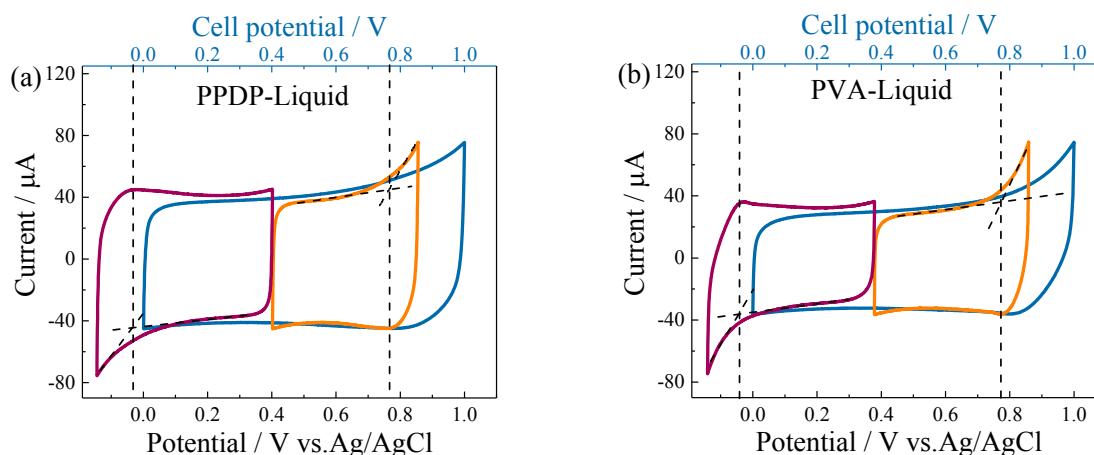
Figure S10. The electrochemical window of graphene-based supercapacitors employing PPDP or PVA liquid electrolyte in a three-electrode in-plane configuration. (a) CV curves of SCs employing liquid PPDP electrolyte. (b) CV curves of SCs employing liquid PVA electrolyte. The cell potential is changed from 0 to 1.0 V and the scan rate is 20 mV s^{-1}.

In Figure S10, the almost constant current with the voltage represents the EDLC behavior, whereas an obvious increase in current as a function of the voltage indicates the occurrence of faradic reactions (i.e., water decomposition). As a result, the upper limit potential (P_{U}) and lower limit potential (P_{L}) of supercapacitors employing PPDP or PVA liquid electrolyte can be determined from the intersection of two straight lines drawn through the CV curves during the transition from the EDLC to the Faradaic behavior.
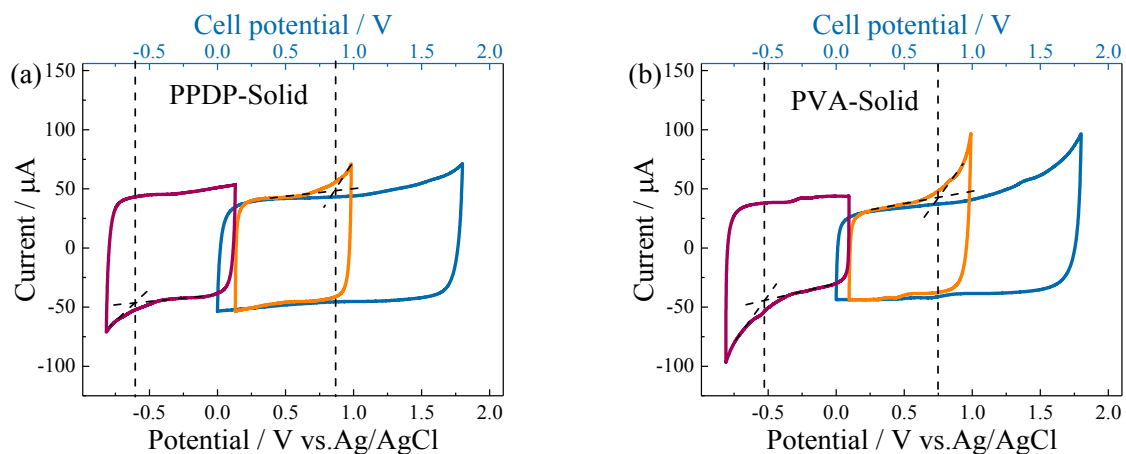
Figure S11. The electrochemical window of graphene-based supercapacitors employing PPDP or PVA gel electrolyte in a three-electrode in-plane configuration. (a) CV curves of SSCs employing PPDP gel electrolyte. (b) CV curves of SSCs employing PVA gel electrolyte. The cell potential is changed from 0 to 1.8 V and the scan rate is 20 mV s^{-1}.

In Figure S11, the upper limit potential (P_U) and lower limit potential (P_L) of supercapacitors employing PPDP or PVA gel electrolyte can be determined from the intersection of two straight lines drawn through the CV curves during the transition from the EDLC to the Faradaic behavior.
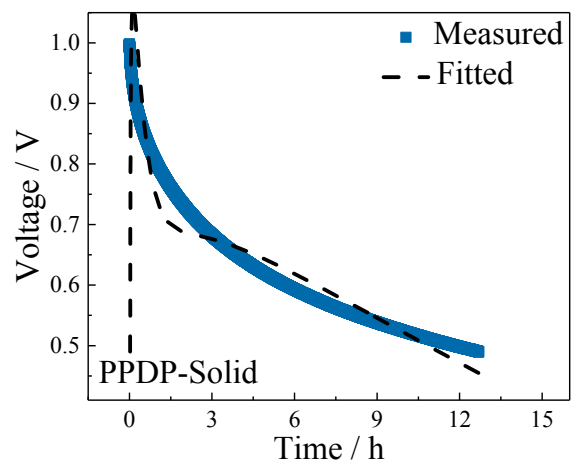
Figure S12. Fitting of the self-discharge curve of SSC employing PPDP gel electrolyte with a model including the contributions of ohmic leakage, diffusion control, and activation control.
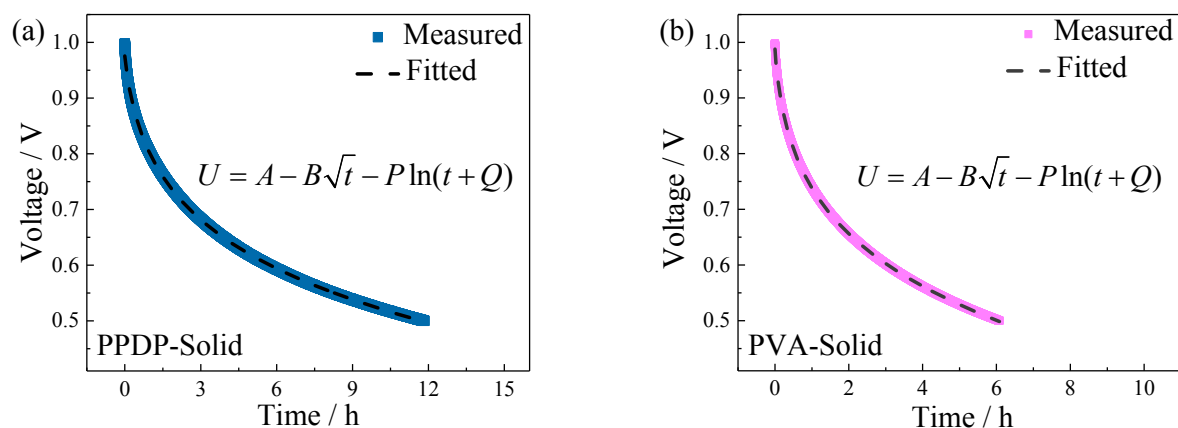
Figure S13. (a) Fitting of the self-discharge curve of SSC employing PPDP gel electrolyte with a model including the contributions of diffusion control and activation control. (b) Fitting of the self-discharge curve of SSC employing PVA gel electrolyte with a model including the contributions of diffusion control and activation control.
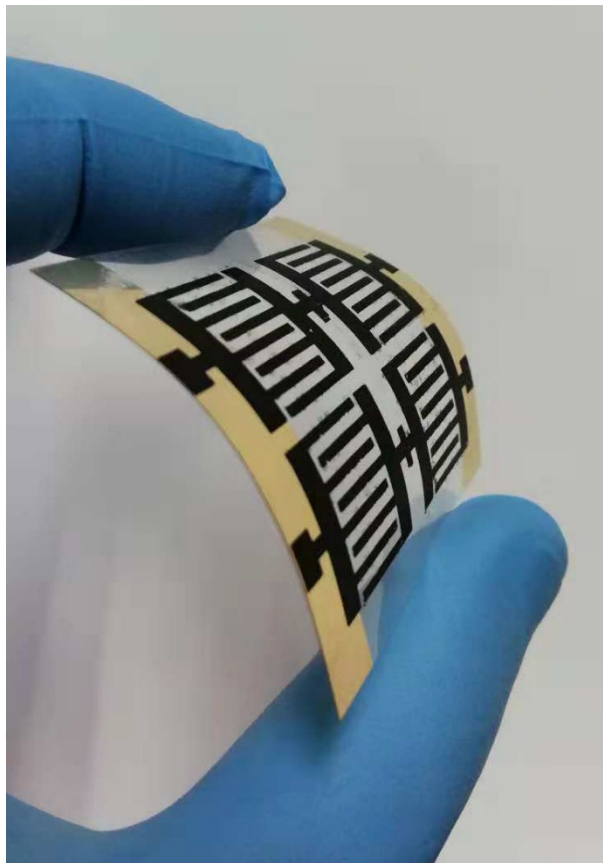
Figure S14. A photograph of interdigital graphene electrode based micro-supercapacitors (MSCs) fabricated by a template filtration method. A gloved hand (in blue) provides a scale.

In Figure S14, PET was used as a substrate and gold was used as current collectors. Here, the configuration of two single SCs in series and then in parallel was applied to power the LCD electronic watches.

Table S1. The ionic conductivities of PPDP and PVA gel electrolytes.

	σ (mS/cm)
PPDP gel electrolyte	~ 6.6
PVA gel electrolyte	~ 2.0

The ionic conductivity for gel polymer electrolytes is determined from the measurement of electrochemical impedance spectroscopy according to the previous studies.[S8,S9] The higher ionic conductivity of the PPDP gel electrolyte than that of the PVA gel electrolyte is an indicative of a faster ion migration in the former than in the later. The fast ion migration would lead to a high specific capacitance at a certain current density. Table S1 shows that the ionic conductivity of the PPDP (M_n of ~ 1.6×10^5 g mol^{-1}) gel electrolyte is ~ 6.6 mS/cm employed for the electrochemical experiments in this work. We have also measured the ionic conductivity of another gel polymer electrolyte sample with a M_n of PPDP of ~ 1.2×10^5 g mol^{-1}. This sample has an ionic conductivity of ~ 8.5 mS/cm. By comparing these two PPDP gel electrolyte samples, we have found that a ~ 33% increase in the molecular weight of PPDP leads to a ~ 22% decrease in the ionic conductivity. Therefore, the PPDP with a lower molecular weight may be more favorable for the movement of ions in the PPDP gel electrolyte.

Table S2. Obtained fitting parameters for the self-discharge of SSCs employing PPDP or PVA gel electrolyte.

	A	B	P	Q
PPDP gel electrolyte	0.86	0.02	0.11	0.34
PVA gel electrolyte	0.80	0.05	0.10	0.15

References

[S1]   X. Peng, H. L. Liu, Q. Yin, J. C. Wu, P. Z. Chen, G. Z. Zhang, G. M. Liu, C. Z. Wu, Y. Xie, *Nat. Commun.* 2016, **7**, 11782.

[S2]   H. A. Andreas, *J. Electrochem. Soc.* 2015, **162**, A5047-A5053.

[S3]   M. Kaus, J. Kowal, D. U. Sauer, *Electrochim. Acta* 2010, **55**, 7516-7523.

[S4]   M. Xia, J. Nie, Z. Zhang, X. Lu, Z. L. Wang, *Nano Energy* 2018, **47**, 43-50.

[S5]   L. Chen, H. Bai, Z. Huang, L. Li, *Energ Environ. Sci.* 2014, **7**, 1750-1759.

[S6]   A. Lewandowski, P. Jakobczyk, M. Galinski, M. Biegun, *Phys. Chem. Chem. Phys.* 2013, **15**, 8692-8699.

[S7]   I. S. Ike, I. Sigalas, S. Iyuke, *Phys. Chem. Chem. Phys.* 2016, **18**, 661-680.

[S8]   X. Yang, F. Zhang, L. Zhang, T. F. Zhang, Y. Huang, Y. S. Chen, *Adv. Funct. Mater.* 2013, **23**, 3353-3360.

[S9]   P. L. Taberna, P. Simon, J. F. Fauvarque, *J. Electrochem. Soc.* 2003, **150**, A292-A300.